Bioinformatic and biochemical analysis of the key binding sites of the pheromone binding protein of *Cyrtotrachelus buqueti* Guerin-Meneville (Coleoptera: Curculionidea)

Hua Yang [Equal first author, 1], **Yan-Lin Liu** [Equal first author, 1], **Yuan-Yuan Tao** [1], **Wei Yang** [Corresp., 1], **Chun-Ping Yang** [1], **Jing Zhang** [2], **Li-Zhi Qian** [1], **Hao Liu** [1], **Zhi-Yong Wang** [3]

[1] Sichuan Agricultural University, Key Laboratory of Ecological Forestry Engineering of Sichuan Province/College of Forestry, Chengdu, Sichuan, China

[2] Provincial Key Laboratory of Agricultural Environmental Engineering, Sichuan Agricultural University, Chengdu, China

[3] Key Laboratory of Control and Resource Development of Bamboo Pest of Sichuan Province, Leshan, China

Corresponding Author: Wei Yang
Email address: ywei0218@aliyun.com

The bamboo snout beetle *Cyrtotrachelus buqueti* is a widely distributed wood-boring pest found in China, and its larvae cause significant economic losses because this beetle targets a wide range of host plants. A potential pest management measure of this beetle involves regulating olfactory chemoreceptors. In the process of olfactory recognition, pheromone-binding proteins (PBPs) play an important role. Homology modeling and molecular docking were conducted in this study for the interaction between CbuqPBP1 and dibutyl phthalate to better understand the relationship between PBP structures and their ligands. Site-directed mutagenesis and binding experiments were combined to identify the binding sites of CbuqPBP1 and to explore its ligand-binding mechanism. The 3D structural model of CbuqPBP1 has six a-helices. Five of these a-helices adopt an antiparallel arrangement to form an internal ligand-binding pocket. When docking dibutyl phthalate within the active site of CbuqPBP1, a CH-π interaction between the benzene ring of dibutyl phthalate and Phe69 was observed, and a weak hydrogen bond formed between the ester carbonyl oxygen and His53. Thus, Phe69 and His53 are predicted to be important residues of CbuqPBP1 involved in ligand recognition. Site-directed mutagenesis and fluorescence assays with a His53Ala CbuqPBP1 mutant showed no affinity toward ligands. Mutation of Phe69 only affected binding of CbuqPBP1 to cedar camphor. Thus, His53(Between α2 and α3) of CbuqPBP1 appears to be a key binding site residue, and Phe69(Located at α3) is a very important binding site for particular ligand interactions.

Bioinformatic and biochemical analysis of the key binding sites of the pheromone binding protein of *Cyrtotrachelus buqueti* Guerin-Meneville (Coleoptera: Curculionidea)

Hua Yang[1¶], Yan-Lin Liu[1¶], Yuan-Yuan Tao[1¶], Wei Yang[1*], Chun-Ping Yang[1], Jing Zhang[2], Li-Zhi Qian[1], Hao Liu[1] and Zhi-Yong Wang[3]

[1] Key Laboratory of Ecological Forestry Engineering of Sichuan Province, College of Forestry, Sichuan Agricultural University, Chengdu, Sichuan 611130, China.

[2] Provincial Key Laboratory of Agricultural Environmental Engineering, Sichuan Agricultural University, Chengdu, Sichuan 611130, China.

[3] Key Laboratory of Control and Resource Development of Bamboo Pest of Sichuan Province, Leshan, Sichuan, 614000, China.

[*]Corresponding Author:

Wei Yang

E-mail: ywei0218@aliyun.com

[¶]These authors contributed equally to this article

18

Abstract

The bamboo snout beetle *Cyrtotrachelus buqueti* is a widely distributed wood-boring pest found in China, and its larvae cause significant economic losses because this beetle targets a wide range of host plants. A potential pest management measure of this beetle involves regulating olfactory chemoreceptors. In the process of olfactory recognition, pheromone-binding proteins (PBPs) play an important role. Homology modeling and molecular docking were conducted in this study for the interaction between CbuqPBP1 and dibutyl phthalate to better understand the relationship between PBP structures and their ligands. Site-directed mutagenesis and binding experiments were combined to identify the binding sites of CbuqPBP1 and to explore its ligand-binding mechanism. The 3D structural model of CbuqPBP1 has six α-helices. Five of these α-helices adopt an antiparallel arrangement to form an internal ligand-binding pocket. When docking dibutyl phthalate within the active site of CbuqPBP1, a CH-π interaction between the benzene ring of dibutyl phthalate and Phe69 was observed, and a weak hydrogen bond formed between the ester carbonyl oxygen and His53. Thus, Phe69 and His53 are predicted to be important residues of CbuqPBP1 involved in ligand recognition. Site-directed mutagenesis and fluorescence assays with a His53Ala CbuqPBP1 mutant showed no affinity toward ligands. Mutation of Phe69 only affected binding of CbuqPBP1 to cedar camphor. Thus, His53(Between α2 and α3) of CbuqPBP1 appears to be a key binding site residue, and Phe69(Located at α3) is a very important binding site for particular ligand interactions.

Keywords: *Cyrtotrachelus buqueti*, pheromone binding protein, bioinformatics, site-directed

39 mutagenesis, fluorescence assay

40

Introduction

During long-term evolution insects have developed a sensitive sense of smell, which enables insects to detect external volatile semiochemicals when searching for various environmental cues, such as foraging for food, finding a breeding partner and locating a spawning ground(Gu et al. 2011; Larsson et al. 2004). Tentacles are the main olfactory part of insects and contain a large variety of receptors. Receptors are widely distributed with various olfactory-rated functional proteins, including odorant binding proteins (OBPs), chemosensory proteins (CSPs) and olfactory receptors (Ors). OBPs are divided into pheromone binding proteins (PBPs), general odorant binding proteins (GOBPs) and antennal binding proteins (ABPs)(Vogt and Riddiford 1981). Research on the binding mechanism between OBPs and ligand molecules has been a major focus of research, including defining the three-dimensional (3D) structure of these OBPs. (Kruse et al. 2003) and (Thode et al. 2008) initially analyzed the general odorant binding protein (LUSH) of *Drosophila melanogaster* and the crystal structure of the complex between LUSH and alcohol, and clarified that Thr57 is a key residue involved in ligand interaction. According to X-ray diffraction analysis of the pheromone binding protein BmorPBP of *Bombyx mori* and structure of bombykol, (Sandler et al. 2000) discovered that Ser56 of this protein played a key role by forming a hydrogen bond with the ligand bombykol. According to the structures of odorant binding protein CquiOBP1 and MOP of *Culex quinquefasciatus*, (Mao et al. 2010) discovered that instead of hydrogen bonds, the interaction between protein and ligand was driven by van der Waals forces and hydrophobic interactions. According to the structure between the

odorant binding protein HoblOBP2 of *Holotrichia oblita* and ethyl benzenecarboxylate, (Zhuang et al. 2013) discovered that this protein-ligand complex involved both van der Waals forces and hydrophobic interactions. Currently, high-resolution structural data describing the complex between the pheromone binding protein of *Cyrtotrachelus buqueti* and an odor molecule is unavailable, and thus information about the mode of action of this protein remains unresolved.

Cyrtotrachelus buqueti (*C. buqueti*) also named as the bamboo snout beetle, belongs to Cyrtotrachelus, Curculionidea, Coleoptera. *C. buqueti* is endangering survival of bamboo shoots from 28 different types of bamboos, including *Bambusa*, *Dendrocalamopsis* and *Dendrocalamus*. The larva, in particular, prefer the bamboo shoots of *Phyllostachys pubescens*, *Dendrocalamopsis oldhami*, *Bambusa textilis*, *Bambusa pervariabilis, Dendrocalamopsis daii* and other sympodial bamboo species(Ju et al. 2005; Wang et al. 2005). *C. buqueti* is distributed widely in the Sichuan Province, Chongqing City, Guangdong Province, Guangxi Province, Guizhou Province and other provinces (districts) as well as Vietnam, Burma, Thailand and other countries and regions in Southeast Asia(Yang et al. 2009). *C. buqueti* is one of 233 hazardous forest pests issued in 2003 for the first time(Yang et al. 2015).

Currently, research on *C. buqueti* has mainly concentrated on a description of the general biological characteristics and common chemical pest control approaches(Ju et al. 2005; Wang et al. 2005; Yang et al. 2010; Yang et al. 2009). The development of sex attractants remains poorly understood. (Mang et al. 2012) have extracted and studied the body surface semiochemicals of *C. buqueti* adults, whereas (Yang et al. 2017a) have constructed a transcriptome library of *C.*

buqueti and analyzed the sex pheromone binding protein gene. (Yang et al. 2017b) have also cloned the sex pheromone binding protein gene that codes for the protein CbuqPBP1, and conducted fluorescence competitive binding assays for many types of simple odor substances. According to the system evolutionary tree，CbuqPBP1 was quite similar to PBP of other insects.Amino acid sequence similarity analysis showed that CbuqPBP1 had 37.68% similarity with 27 PBPs of 17 insects of Coleoptera and Lepidoptera. The similarities with Coleoptera and Lepidoptera were 38.47% and 52.39% respectively.(Yang et al., 2018).

In this paper, homology modeling of the pheromone binding protein CbuqPBP1 of *C. buqueti* has been conducted to create a 3D model of the protein. Molecular docking has also been carried out to define the interaction mode between the ligand dibutyl phthalate and CbuqPBP1. Two key binding site residues, Phe69 and His53, were identified from this modeling and were mutated. Fluorescence competitive binding assays were conducted for these mutants and binding mechanism between CbuqPBP1 and odor molecules were analyzed. The results provide a platform for using pheromones to prevent and control *C. buqueti* efficiently.

Materials & Methods

Materials

Three compounds were used to investigate the ligand-binding specificity of CbuqPBP1. Ligands of the highest purity were purchased from Aladdin (Shanghai, China) and stored according to the

manufacture's specifications. The sequence of CbuqPBP1 was taken from the GenBank with accession number KU845733.1.

Alignment and homology modeling

The amino acid sequence of CbuqPBP1 was downloaded from the GenBank and Blast was used to search against the CbuqPBP1 protein sequence in the Protein Data Bank to identify a structural template. Software Modeller 9.19 (http://salilab.org/modeller/) was used for homology modeling based on the sequence comparison results with the structural template sequence identified. The 3D structure obtained from modeling was evaluated with SAVES v5.0 (https://servicesn.mbi.ucla.edu/SAVES/). After confirmation of the models, the Chiron (http://redshift.med.unc.edu/chiron/login.php) on-line server was used for optimization. Modeller 9.19 was used to optimize loop regions and PyMOL was used to analyze structural characteristics and to search for ligand binding sites.

Molecular docking

Based on the established homology model, the docking program AUTODOCK vina 1.1.2 was used to find the potential binding mode between CbuqPBP1 and the ligand dibutyl phthalate. Dibutyl phthalate with strong affinity is a female pheromone of the giant bamboo weevil, which plays a role in the process of male individual searching for female individual. ChemBioDraw Ultra 14.0 was used to simulate the structure of dibutyl phthalate and to generate a 3D structure of the ligand. Energy optimization was conducted using the MMFF94 force field and Autodock

Tools 1.5.6 was used to create the PDBQT format(Huey et al. 2007; Morris et al. 2009). Binding coordinates of CbuqPBP1 and dibutyl phthalate were set to: center_x = 22.389, center_y = –25.143, center_z = 1.08, and size_x = 15, size_y = 15, size_z = 15. Parameter exhaustiveness was set to 20 and default values were used for other parameters to increase the calculation accuracy. Finally, the conformation with the highest score was selected and PyMoL 1.7.6 was used for visual inspection and analysis of the structural data.

Site-directed mutagenesis

The CbuqPBP1 coding sequence was mutated to yield the two mutants CbuqPBP1-Phe69A (phenylalanine to alanine at position 69) and CbuqPBP1-His53A (histidine to alanine at position 53). PCR reactions were used to form overlapping chains. The extension of overlapping chains was used to splice segments in a superimposed manner. Primer5 was used to design primers (Table 1). Three rounds of PCR amplification were conducted after designing primers. Expression vectors (pET-28a(+)/PBP1-Phe69A, pET-28a(+)/PBP1-His53A and pET-28a(+)/PBP1) were generated and transformed into *Escherichia coli* BL21(DE3) competent cells for protein overexpression. Recombinant proteins produced were detected by SDS-PAGE analysis.

Expression and purification of the native protein and mutants

Expression plasmids were transformed into *E. coli* TOP10 competent cell and plated on agar plates. Several colonies were selected randomly for overnight cultivation in LB media and

plasmids were extracted for sequencing. Mutant plasmids pET-28a(+)/PBP1- Phe69A and pET-28a(+)/PBP1- His53A with the correct sequence were transformed into *E. coli* BL21(DE3) competent cells, and cells were grown to an optical density at 600 nm (OD_{600}) of 0.6. IPTG was added to the culture to a final concentration of 1 mM and cells were further grown at 37 ℃ with shaking for 3 h to induce protein expression(Deng et al. 2011). After harvesting cells by centrifugation, ultrasound sonication was used to disrupt cells (200 W, 3/4 s, 25–30 min). The supernatants and sediments were collected under low temperature centrifugation (16000 g-force, 50 min) and SDS-PAGE detection was conducted. Nickel affinity (Ni-NTA) was used to purify recombination proteins, and the purified proteins were stored in Tris-HCl buffer (pH 7.4, 50 mM). To avoid the function of the protein being affected by the His-tag, recombinant bovine enterokinase was used to remove the His-tag and the protein was re-purified and collected. Purity was confirmed by SDS-PAGE analysis.

Fluorescence assay

To measure the affinity of the fluorescent ligand N-phenyl-1-naphthylamine (1-NPN) toward CbuqPBP1, a 2 μM solution of protein in 50 mM Tris–HCl, pH 7.4, was titrated with aliquots of 1 mM 1-NPN dissolved in methanol to a final concentration of 16 μM. The probe was excited at 337 nm and emission spectra were recorded between 350 and 550 nm. To evaluate the effect of pH on the binding affinity of CbuqPBP1, we also measured its binding with 1-NPN over a pH range of 4.5–9.0. The displacement of 1-NPN by selected ligands was measured in a competitive binding assay using both the protein and 1-NPN at 2 μM. The mixtures were titrated with 1 mM

158 methanol solutions of each competitor at concentrations of 2–16 μM. The fluorescence of the
159 mixture was recorded after 5 min. Dissociation constants for 1-NPN and the stoichiometry of
160 binding were obtained from Scatchard plots of the binding data using the Prism software. For
161 other competitor ligands, the dissociation constants were calculated from the corresponding half
162 maximal inhibitory concentration (IC_{50}) values using the equation: inhibitory constant Ki =
163 $[IC_{50}]/(1 + [1\text{-NPN}]/K_{1\text{-NPN}})$, where [1-NPN] is the free concentration of 1-NPN and $K_{1\text{-NPN}}$ is the
164 dissociation constant of the protein/1-NPN complex.

165

166 **Results**

167 **Three-dimensional model of CbuqPBP1**

168 According to the Blast search against the Protein Data Bank, two types of insect odor proteins
169 with known structures and quite similar sequences to the CbuqPBP1 sequence were found. These
170 two odorant binding proteins were *Nasonovia ribisnigri* OBP3 (NribOBP3 PDB ID: 4Z45_A)
171 and *Megoura viciae* OBP3 (MvicOBP3 PDB ID: 4Z39_A). The total sequence identity between
172 the target (CbuqPBP1) and the template protein (NribOBP3) is 33% (Cavasotto and Phatak
173 2009)(Fig. 1A). The resolution of the template is 2.02 Å.

174 After homology modeling, the 3D structure of CbuqPBP1 (Fig. 1B) is clearly very similar
175 to the 3D structure of the template NribOBP3 (Fig. 1C). The structural characteristics of
176 CbuqPBP1 are similar to other sex pheromone binding proteins and include six α-helices:

177 residues 26–36 (α1), 44–51 (α2), 59–72 (α3), 83–94 (α4), 101–114 (α5) and 123–137 (α6). Six
178 conserved cysteine residues stabilize the protein structure by forming three disulfide bonds.
179 Disulfide bond Cys36–Cys67 connects α1 and α3, Cys63–Cys121 connects α3 and α6, and
180 Cys110–Cys130 connects α5 and α6. Five of the α-helices adopt an antiparallel arrangement
181 (α1, α3, α4, α5 and α6) and form an internal binding pocket. α2 forms a cover-type structure or
182 lid above the pocket, which stabilizes this structure.

183 The result of further rationality estimates by Pro-CHECK (Fig. 1D) was that 88.4% residues
184 were in the favored regions (red area A, B and L), 10.1% of the residues fall into additionally
185 allowed regions (bright yellow area a, b, l, p) and 0.8% residues have backbone torsion angles
186 that fall into generously allowed regions (light yellow area ~a, ~b, ~l, ~p). The percentage sum
187 of residues in the allowed regions was 99.3%, which was higher than 95%. This result showed
188 that the constructed 3D structure of CbuqPBP1 was a high-quality model.

189 Energy assessment was performed on ProSa（Fig. 1E）.The shadow part is Z-score value
190 of all proteins similar to Cbuq PBP1 protein in PDB database, and the black spot is Z-score value
191 of Cbuq PBP1 protein, which is -4.35. The Z-score value of template protein NOBP3 is -5.87 in
192 the range of Z-score of known reasonable structural proteins, which indicates that the modeling
193 structure is more stable than template structure. This indicates that the homologous modeling
194 Institute is more stable than template structure. The constructed CBuq PBP1 protein is
195 reasonable in energy.

196 **Molecular docking**

197 To research characteristics of CbuqPBP1 binding with odor molecules, dibutyl phthalate
198 (Fig. 2A), which interacts with CbuqPBP1 favorably, was selected to construct a complex
199 between CbuqPBP1 3D model and dibutyl phthalate. Such a model should clarify the mode of
200 interaction of dibutyl phthalate with CbuqPBP1 at the molecular level. We have docked dibutyl
201 phthalate with the active pocket of CbuqPBP1, with a binding energy of –6.4 kcal/mol.
202 Generally, compound dibutyl phthalate bound to the active pocket of CbuqPBP1 with a compact
203 conformation (Fig. 2B).

204 The benzene ring and one aliphatic chain of dibutyl phthalate were located in the
205 hydrophobic region at the bottom of the pocket. Strong hydrophobic interactions formed between
206 the ligand and residues Leu3, Leu4, Leu5, Leu29, Leu50, Pro56, Ile65 and Phe69. Another side
207 chain of dibutyl phthalate was located at the opening of the pocket. According to detailed
208 analysis, a CH-π interaction may occur between the benzene ring of dibutyl phthalate and residue
209 Phe69. Moreover, an important long-range hydrogen bond (3.3 Å) can form between one ester
210 carbonyl oxygen of dibutyl phthalate and residue His53 (Fig. 2C). All aforementioned
211 interactions enable the formation of a stable complex between dibutyl phthalate and CbuqPBP1.

212 **Site-directed mutagenesis of CbuqPBP1 and binding specificities of mutants**

213 After double enzyme digestion with restriction enzymes *Nde* I and *Xha* I, mutant plasmids pET-
214 28a(+)/CbuqPBP1-His53A and pET-28a(+)/CbuqPBP1-Phe69A, and the original plasmid pET-
215 28a(+)/PBP1 formed bands in an agarose gel that were ~400 bp in length (Fig. 3). After SDS-
216 PAGE analysis of protein overexpression, three specific bands with molecular weights of 16 kDa

were observed in the SDS-PAGE gel, which is consistent with expected molecular weight of the target proteins (Fig. 4).

After ultrasonication to disrupt the bacteria and release the recombinant proteins (including His tag), SDS-PAGE analysis could be conducted (Fig. 5). All recombinant proteins were found in the supernatant part of the disrupted cells. After purification, recombinant bovine enterokinase was used to cleave the His-tag and following a further round of purification pure recombinant protein samples were obtained.

1-NPN was selected as the fluorescent probe. Fluorescence competitive binding assays were conducted for the purified wild-type CbuqPBP1 and mutant CbuqPBP1-His53A and CbuqPBP1-Phe69A proteins. The fluorescence peak maximum in the presence of the recombinant proteins was recorded at different concentrations. The Scatchard equation was used to calculate the equilibrium binding constant (K_d) between CbuqPBP1, CbuqPBP1-His53A, CbuqPBP1-Phe69A and 1-NPN, which were determined to be 2.725, 3.352 and 2.260 μM, respectively. When the final concentration of odor substance was higher than 50 μM, the fluorescence peak did not decrease to half its value. This showed that almost no affinity was established between protein and the odor substance, and the binding constant could not be calculated (Fig. 6).

Dibutyl phthalate, benzothiazole and cedar camphor were selected based on previous fluorescence binding assay test(Yang et al. 2017b). Fluorescence competitive binding assays were conducted with CbuqPBP1, CbuqPBP1-His53A and CbuqPBP1-Phe69A (Fig. 7). According to the results, CbuqPBP1 bound favorably with dibutyl phthalate, benzothiazole and

237 cedar camphor. The binding ability of CbuqPBP1-His53A with the three types of odor
238 substances was essentially lost. The binding ability of CbuqPBP1-Phe69A mutant with cedar
239 camphor was significantly reduced, whereas affinity toward the other two odor substances was
240 not significantly different from that of the wild-type protein (Table 2).

241

242 **Discussion**

243 Currently, 3D structure prediction of odorant binding proteins through homology modeling has
244 been conducted for proteins from *Choristoneura rosaceana, Choristoneura murinana,*
245 *Pectinophora gossypiella, Heliothis assulta, Spodoptera exigua, Spodoptera exigua, Holotrichia*
246 *oblita, lettuce Aphidoidea, Megoura viciae* and other insects(Northey et al. 2016; Sun et al. 2013;
247 Wang et al. 2015). According to homology modeling of pheromone binding protein CbuqPBP1
248 of *C. buqueti*, the 3D structure is composed of six α-helices, which packed together and were
249 stabilized by three disulfide bonds. Disulfide bond Cys36–Cys67 connected α1 and α3, Cys63–
250 Cys121 connected α3 and α6, and Cys110–Cys130 connected α5 and α6. Five of the α-helices
251 arranged in an antiparallel manner to form an internal binding pocket(Tian et al. 2017). α2
252 formed a cover-type structure above the pocket, which was similar to *Holotrichia oblita*
253 HoblOBP2(Zhuang et al. 2013) structures. As for 3D structure of *Bombyx mori* BmorPBP, four
254 antiparallel α-helices formed a hydrophobic pocket and α2 and α3 did not participate in the
255 formation of the pocket(Sandler et al. 2000). This might be due to differences in hydrophobic
256 pocket of the 3D structure of odorant binding proteins from different insects. Such differences

257 are likely to be closely related to the function of these proteins.

258 According to research, odorant binding proteins from some insects interact with their
259 cognate ligand through hydrogen bonds and hydrophobic interactions, whereas other odorant
260 binding proteins from other insects interact with odorants via van der Waals forces and
261 hydrophobic interactions(Sandler et al. 2000). In this report, a CH-π interaction formed between
262 the benzene ring of dibutyl phthalate and Phe69. This CH-π interaction is generally considered to
263 be a relatively weak hydrogen bond.

264 Previous research has indicated that CH-π interactions are important in carbohydrate–
265 protein identification processes, where the CH-π features as a synergistic interaction that plays an
266 important role in stabilizing the structure of the complex (Jiang et al. 2009; Kozmon et al. 2011).
267 The CH-π interaction involves a nonpolar interaction between the CH proton and electron-rich
268 aromatic ring π electron cloud system, playing a similar role to hydrogen bonding in controlling
269 crystal stacking, maintaining biomolecular structures and participating in molecular recognition
270 processes(Ye et al. 2015; Zhao et al. 2014). Therefore, we hypothesize that the CH-π interaction
271 may play a role in binding and stabilizing the interaction with odor molecules.

272 An ester carbonyl oxygen from dibutyl phthalate and His53 from the protein formed a weak
273 3.3 Å hydrogen bond. Such a hydrogen bond has been reported in odorant binding proteins of
274 other insects, for example, BmorPBP1 of *B. mori* and pheromone compound interacted through a
275 hydrogen bond. General odorant binding protein (LUSH) from *Drosophila melanogaster* and the
276 pheromone binding protein (ApolPBPl) from *Antheraea polyphemus* interact with their cognate

277 ligands through hydrogen bonds(Damberger et al. 2007; Thode et al. 2008). Therefore, we
278 hypothesized that the CbuqPBP1 interaction and release of the ligand involves hydrogen bond
279 formation via His53.

280 According to the fluorescence competitive binding assay, mutant pET-28a(+)/PBP1-His53A
281 could not interact with odor substances. Replacing His53 with alanine removed the ability of the
282 mutant to form this key hydrogen bond with ligands, and therefore the ability to bind with odor
283 substances. Thus, His53 is a key binding site residue of the pheromone binding protein of *C.*
284 *buqueti*. Mutein pET-28a(+)/PBP1-Phe69A did not bind cedar camphor. However, only a
285 decrease in binding ability toward dibutyl phthalate and benzothiazole was observed. These
286 observations indicate that only a small number of intermolecular forces between the protein and
287 odor molecules were affected by this mutation(Zhuang et al. 2014). Thus, the binding affinity
288 had been reduced, but not completely lost. Therefore, Phe69 is the binding site for CbuqPBP1 to
289 combine with odor substance; however, Phe69 is not a key binding site residue. Moreover, these
290 observations showed that the combination between CbuqPBP1 and ligands was affected by loss
291 of hydrogen bonding and other intermolecular forces, and the interaction between CbuqPBP1
292 and ligands involves the joint action of many acting forces and the binding site(Li et al. 2016).

293 **Acknowledgments**

294 This work was funded by the key fund of the education department in Sichuan (17ZB0344) and
295 the key laboratory fund for scientific research in Sichuan (003Z1401). The experiments were
296 conceived and coordinated by HY, YYT, YLL, WY, ZYW ,LZQ and CPY. Sampling was

297 performed by HY, YLL and YYT. Molecular docking was performed by HY, YLL, HL and JZ.
298 HY, YLL and WY drafted the manuscript. All authors read and approved the final version of the
299 manuscript submitted for publication. The authors thank Liwen Bianji, Edanz Editing China
300 (www.liwenbianji.cn/ac), for editing the English text of a draft of this manuscript.
301

302 **Figure legends**

303 **Figure 1 Three-dimensional (3D) model of CbuqPBP1.** (A) Sequence alignment between
304 CbuqPBP1 and NribOBP3. (B) 3D structure of CbuqPBP1. The N and C termini and the six α-
305 helices are labeled and the three disulfide linkages are shown in yellow stick representations. (C)
306 Superimposed penetrative structure of CbuqPBP1 and NribOBP3. The model of CbuqPBP1 and
307 crystal structure of NribOBP3 are shown in green and violet, respectively. (D) The results of the
308 PROCHECK evaluation of the CbuqPBP1 model. (E) Overall model quality.

309 **Figure 2 The binding pocket of CbuqPBP1 and the docking result with dibutyl phthalate.**
310 (A) Tertiary structure of dibutyl phthalate. (B) The binding pocket of CbuqPBP1 and dibutyl
311 phthalate docked into the active site of the CbuqPBP1 receptor. (C) Diagram of the van der
312 Waals interactions and hydrophobic interactions of dibutyl phthalate with key binding site
313 residues.

314 **Figure 3 Double digestion map of the mutant and wild-type plasmids.** Lane Marker: protein
315 molecular weight standard; Lane 1: pET-28a (+)/PBP1-Phe69A; Lane 2: pET-28a (+)/PBP1-
316 His53A; and Lane 3: pET-28a (+)/PBP1.

317 **Figure 4 SDS-PAGE analysis of the total bacterial protein lysate of the mutant and wild-**
318 **type CbuqPBP1.** (A) CbuqPBP1-His53A mutant. Lane 1: IPTG induced total protein lysate;
319 Lane 2: total protein lysate without IPTG induction. (B) CbuqPBP1- Phe69A mutant. Lane 1:
320 total protein lysate without IPTG induction; Lane 2: IPTG induced total protein lysate. (C) wild-

type CbuqPBP1. Lane 1: IPTG induced total protein lysate; Lane 2: total protein lysate without IPTG induction.

Figure 5 SDS-PAGE analysis of supernatant and precipitant of bacterial fragmentation following expression of the mutant and wild-type CbuqPBP1. Lane 1: IPTG induced expression of insoluble material; Lane 2: IPTG induced expression of supernatant following cell disruption by sonication. (A) wild-type protein. (B) CbuqPBP1-His53A mutant. (C) CbuqPBP1-Phe69A mutant.

Figure 6 The binding curve and K_d of mutant and wild-type CbuqPBP1 toward 1-NPN. (A) wild-type protein. (B) CbuqPBP1-His53A mutant. (C) CbuqPBP1- Phe69A mutant.

Figure 7 Competitive binding curves of selected ligands toward mutant and wild-type CbuqPBP1. (A) wild-type protein. (B) CbuqPBP1-His53A mutant. (C) CbuqPBP1- Phe69A mutant.

Reference

Cavasotto, C.N., and S.S. Phatak. 2009. Homology modeling in drug discovery: current trends and applications. Drug Discov Today 14: 676-683.

Damberger, F.F., Y. Ishida, W.S. Leal and K. Wuthrich. 2007. Structural basis of ligand binding and release in insect pheromone-binding proteins: NMR structure of Antheraea polyphemus PBP1 at pH 4.5. J Mol Biol 373: 811-819.

Deng, S.S., J. Yin, T. Zhong and Y.Z. Cao. 2011. Function and immunocytochemical localization of two novel odorant-binding proteins in olfactory sensilla of the scarab beetle *Holotrichia oblita* Faldermann (Coleoptera: Scarabaeidae). Chemical Senses 37: 141-150.

342 Gu, S.H., S.P. Wang, X.Y. Zhang, K.M. Wu, Y.Y. Guo, J.J. Zhou and Y.J. Zhang. 2011. Identification and tissue
343 distribution of odorant binding protein genes in the lucerne plant bug Adelphocoris lineolatus (Goeze). Insect
344 Biochem Mol Biol 41: 254-263.

345 Huey, R., G.M. Morris, A.J. Olson and D.S. Goodsell. 2007. A semiempirical free energy force field with charge-
346 based desolvation. J Comput Chem 28: 1145-1152.

347 Jiang, Q.Y., W.X. Wang, Z. Zhang and L. Zhang. 2009. Binding specificity of locust odorant binding protein and its
348 key binding site for initial recognition of alcohols. Insect Biochem Mol Biol 39: 440-447.

349 Ju, R.T., C.H. Xiao, J.H. Xu, Y. Xu, X.Z. Chi and Y.Z. Li. 2005. *Cyrthotrachelus buqueti* in Shanghai. Forest Pest and
350 Disease 24: 7-9.

351 Kozmon, S., R. Matuska, V. Spiwok and J. Koca. 2011. Dispersion interactions of carbohydrates with condensate
352 aromatic moieties: theoretical study on the CH-pi interaction additive properties. Phys Chem Chem Phys 13:
353 14215-14222.

354 Kruse, S.W., R. Zhao, D.P. Smith and D.N. Jones. 2003. Structure of a specific alcohol-binding site defined by the
355 odorant binding protein LUSH from Drosophila melanogaster. Nat Struct Biol 10: 694-700.

356 Larsson, M.C., A.I. Domingos, W.D. Jones, M.E. Chiappe, H. Amrein and L.B. Vosshall. 2004. Or83b encodes a
357 broadly expressed odorant receptor essential for Drosophila olfaction. Neuron 43: 703-714.

358 Li, Y.H., P.Y. Deng, Y.M. Liu and Z.H. Lei. 2016. Binding mechanisms of sex pheromone with pheromone binding and
359 receptor proteins in *Plutella xylostella*. Journal of Southern Agriculture 47: 928-933.

360 Mang, D.Z., Q.H. Luo, M. Shu and W. Wei. 2012. Extraction and identification of cuticular semiochemical
361 components of *Cyrtotrachelus buqueti* Guerin-Meneville (Coleoptera: Curculionidae). Acta Entomol Sin 55: 291-302.

362 Mao, Y., X. Xu, W. Xu, Y. Ishida, W.S. Leal, J.B. Ames and J. Clardy. 2010. Crystal and solution structures of an
363 odorant-binding protein from the southern house mosquito complexed with an oviposition pheromone. Proc Natl
364 Acad Sci U S A 107: 19102-19107.

365 Morris, G.M., R. Huey, W. Lindstrom, M.F. Sanner, R.K. Belew, D.S. Goodsell and A.J. Olson. 2009. AutoDock4 and
366 AutoDockTools4: Automated docking with selective receptor flexibility. J Comput Chem 30: 2785-2791.

367 Northey, T., H. Venthur, F. De Biasio, F.X. Chauviac, A. Cole, K.A.J. Ribeiro, G. Grossi, P. Falabella, L.M. Field, N.H.
368 Keep and J.J. Zhou. 2016. Crystal Structures and Binding Dynamics of Odorant-Binding Protein 3 from two aphid
369 species Megoura viciae and Nasonovia ribisnigri. Sci Rep 6: 24739.

370 Sandler, B.H., L. Nikonova, W.S. Leal and J. Clardy. 2000. Sexual attraction in the silkworm moth: structure of the

371 pheromone-binding-protein-bombykol complex. Chem Biol 7: 143-151.

372 Sun, H., L.X. Zhao, F.R. Zhou and H. Gao. 2013. Pheromone binding protein of *Helicoverpa zea* based on Homology
373 modeling. Ningxia Journal of Agriculture and Forestry Science and Technology 54: 37-39.

374 Thode, A.B., S.W. Kruse, J.C. Nix and D.N. Jones. 2008. The role of multiple hydrogen bonding groups in specific
375 alcohol binding site in protein: Insights from structural studies of LUSH. Journal of Molecular Biology 376: 1360-
376 1376.

377 Tian, Z.Q., L.N. Sun, Y.Y. Li, H.J. Zhang, W.T. Yan, Q. Yue, L.F. Quan and G.S. Qiu. 2017. Research progress of the
378 function of sex pheromone binding protein in insects. Journal of Agriculture 7: 14-20.

379 Vogt, R.G., and L.M. Riddiford. 1981. Pheromone binding and inactivation by moth antennae. Nature 293: 161-163.

380 Wang, W.D., F.Z. Chen and X.Q. Wang. 2005. Reproductive behavior of *Cyrtotrachelus buqueti*. Sichuan J Zool 24:
381 540-541.

382 Wang, Y., H. Sun, J.Y. Zhu, N. Zhao and B. Yang. 2015. Homology modeling of the odorant binding protein of the
383 pine shoot beetle, *Tomicus yunnanensis*. Chinese Journal of Applied Entomology 54: 1223-1228.

384 Yang, H., T. Su, W. Yang, C. Yang, L. Lu and Z. Chen. 2017a. The developmental transcriptome of the bamboo snout
385 beetle *Cyrtotrachelus buqueti* and insights into candidate pheromone-binding proteins. PLoS One 12: e0179807.

386 Yang, H., T. Su, W. Yang, C.P. Yang, Z.M. Chen, L. Lu, Y.L. Liu and Y.Y. Tao. 2017b. Molecular characterization,
387 expression pattern and ligand-binding properties of the pheromone-binding protein gene from *Cyrtotrachelus*
388 *buqueti*. Physiol Entomol 42: 1-10.

389 Yang, H., T. Su, W. Yang, C.P. Yang, X.L.Zhou and Y. P. Li 2018. Molecular Cloning and Expression Analysis of
390 CbuqPBP1 Gene in the Bamboo Snout Beetle,Cyrtotrachelus buqueti. Journal of Sichuan Agricultural University
391 36:78-85.

392 Yang, H., W. Yang, C.P. Yang, Y. Cai, Y.F. Pu, Y.W. Fu and Z.R. He. 2015. Mating behavior of *Cyrtotrachelus buqueti*
393 (Coleoptera: Curculionidae). Acta Entomol Sin 58: 60-67.

394 Yang, Y.J., H. Qin, S.F. Wang, Y.P. Wang, H. Liao and S.G. Li. 2010. Antennal ultrastructure and electroantennogram
395 responses of *Cyrtotrachelus buqueti* Guerin-Meneville (Coleoptera: Curculionidae) to volatiles of bamboo shoot.
396 Acta Entomol Sin 53: 1087-1096.

397 Yang, Y.J., S.F. Wang, J.W. Gong, C. Liu, C. Mu and H. Qin. 2009. Relationships among *Cyrtotrachelus buqueti* larval
398 density and wormhole number and bamboo shoot damage degree. Chinese J Appl Ecol 20: 1980-1985.

399 Ye, Y.X., J.J. Liang, H.P. Wang, Z. Meng, X.D. Zhang and L.X. Xu. 2015. Noncovalent surface functionalization of

400 multi-walled carbon nanotubes with polyhedral oligomeric silsesquioxane nanoparticles based on CH-π
401 interactions. Acta Polymerica Sinica 4: 427-436.

402 Zhao, C., P. Li, M.D. Smith, P.J. Pellechia and K.D. Shimizu. 2014. Experimental study of the cooperativity of CH-π
403 interactions. Org Lett 16: 3520-3523.

404 Zhuang, X., Q. Wang, B. Wang, T. Zhong, Y. Cao, K. Li and J. Yin. 2014. Prediction of the key binding site of odorant-
405 binding protein of Holotrichia oblita Faldermann (Coleoptera: Scarabaeida). Insect Mol Biol 23: 381-390.

406 Zhuang, X.J., J. Yin, K.B. Li and Y.Z. Cao. 2013. Bioinformatics analysis of the odorant-binding protein HoblOBP2 in
407 olfactory sesilla of the scarab beetle *Holotrichia oblita*. Plant Protection 39: 50-55.

408

409

Table 1(on next page)

Mutagenic primers for CbuqPBP1

Primers	Sequence
PBP1-F69A-Fm	5’-aatgcactattttctgtacagcgaaaaaattcgatttgatgaaag-3’
PBP1-F69A-Rm	5’-ctttcatcaaatcgaatttttttcgctgtacagaaaatagtgcatt-3’
PBP1-H53A-Fm	5’-gatatccaagctctgatgaacgcggaacgaccagtcacccatgc-3’
PBP1-H53A-Rm	5’-gcatgggtgactggtcgttccgcgttcatcagagcttggatatc-3’
PBP1-F	5’-ggaattccatatgcttagcgaaagcttagttgttgatg-3’
PBP1-R	5’-ccgctcgagttaaaaactggtaattccaag-3’

1

2

Table 2(on next page)

Binding ability of ligands to mutant and wild-type CbuqPBP1

Ligands	IC50 (μM)			Ki (μM)		
	PBP1	H53A	F69A	PBP1	H53A	F69A
benzothiazole	13.426	–	10.538	9.822	–	7.305
dibutyl phthalate	16.889	–	20.04	12.355	–	13.893
cedrol	29.953	–	–	21.912	–	–

1

2

Figure 1

Three-dimensional (3D) model of CbuqPBP1

(A) Sequence alignment between CbuqPBP1 and NribOBP3. (B) 3D structure of CbuqPBP1. The N and C termini and the six a-helices are labeled and the three disulfide linkages are shown in yellow stick representations. (C) Superimposed penetrative structure of CbuqPBP1 and NribOBP3. The model of CbuqPBP1 and crystal structure of NribOBP3 are shown in green and violet, respectively. (D) The results of the PROCHECK evaluation of the CbuqPBP1 model. (E) Overall model quality.

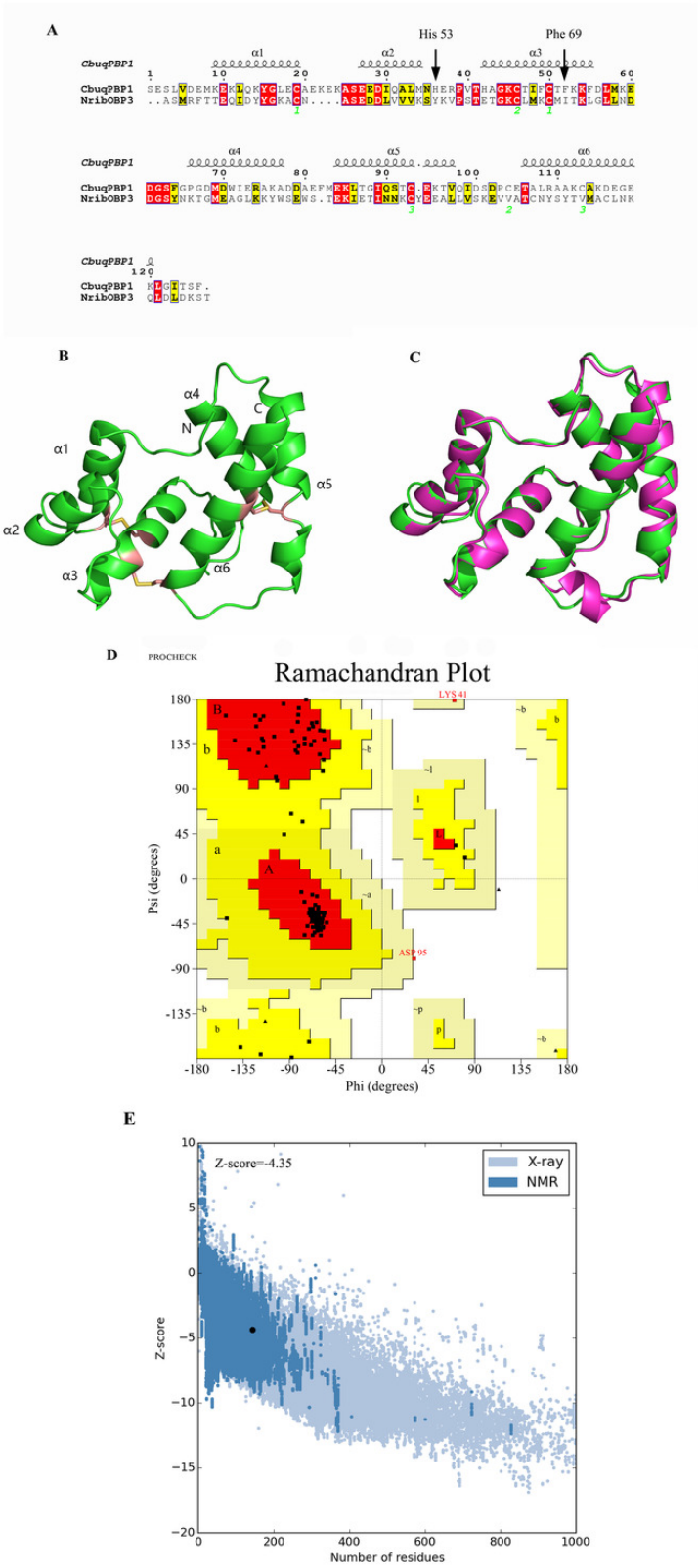
A
His 53
Phe 69
CbuqPBP1
NribOBP3
B
C
α1
α2
α3
α4
α5
α6
N
C
D
PROCHECK
Ramachandran Plot
Psi (degrees)
Phi (degrees)
LYS 41
ASP 95
E
Z-score=-4.35
X-ray
NMR
Z-score
Number of residues

Figure 2

The binding pocket of CbuqPBP1 and the docking result with dibutyl phthalate

(A) Tertiary structure of dibutyl phthalate. (B) The binding pocket of CbuqPBP1 and dibutyl phthalate docked into the active site of the CbuqPBP1 receptor. (C) Diagram of the van der Waals interactions and hydrophobic interactions of dibutyl phthalate with key binding site residues.

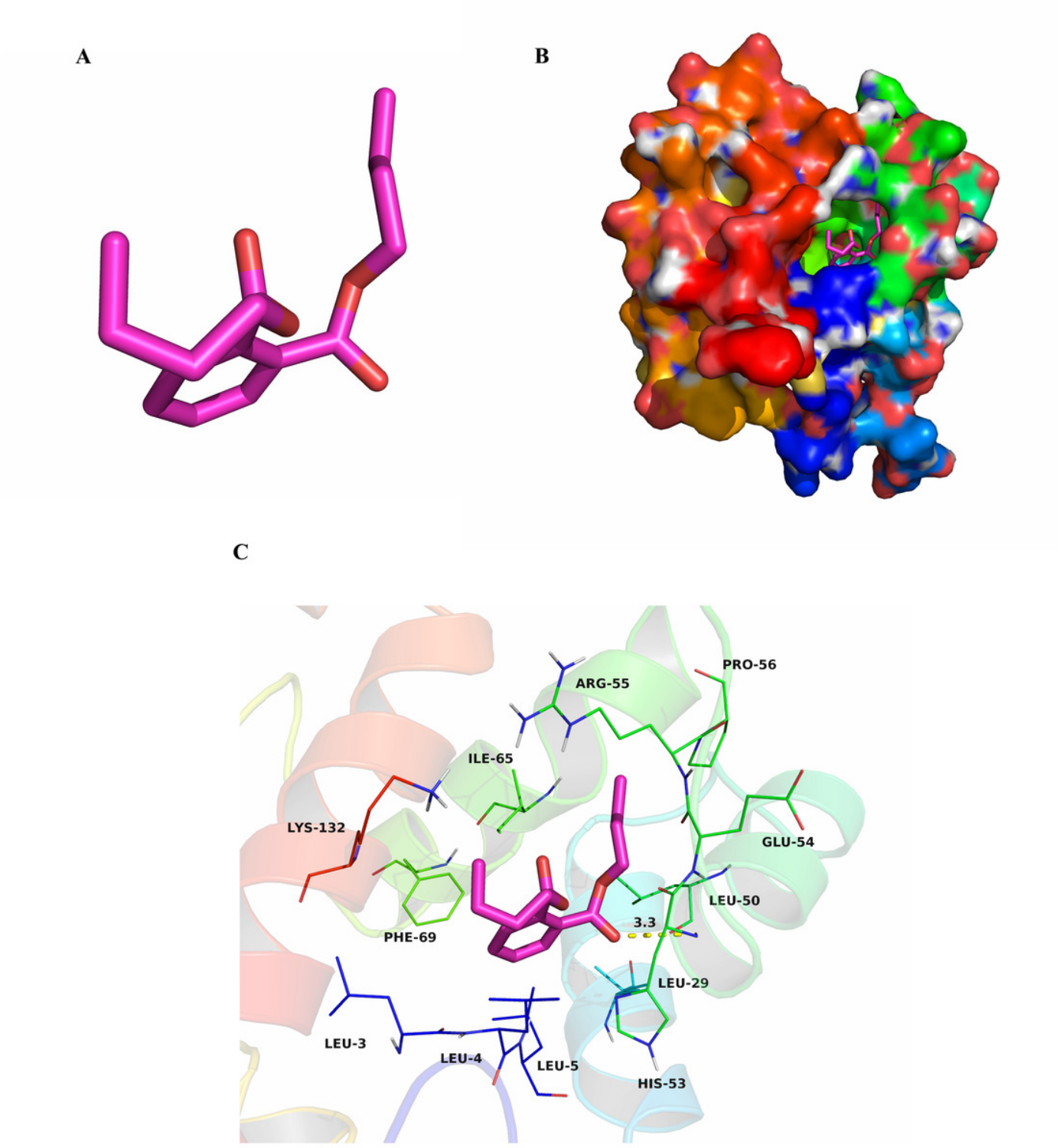
A
B
C
ARG-55
PRO-56
ILE-65
LYS-132
GLU-54
LEU-50
3.3
PHE-69
LEU-29
LEU-3
LEU-4
LEU-5
HIS-53

Figure 3

Double digestion map of the mutant and wild-type plasmids

Lane Marker: protein molecular weight standard; Lane 1: pET-28a (+)/PBP1-Phe69A; Lane 2: pET-28a (+)/PBP1-His53A; and Lane 3: pET-28a (+)/PBP1.

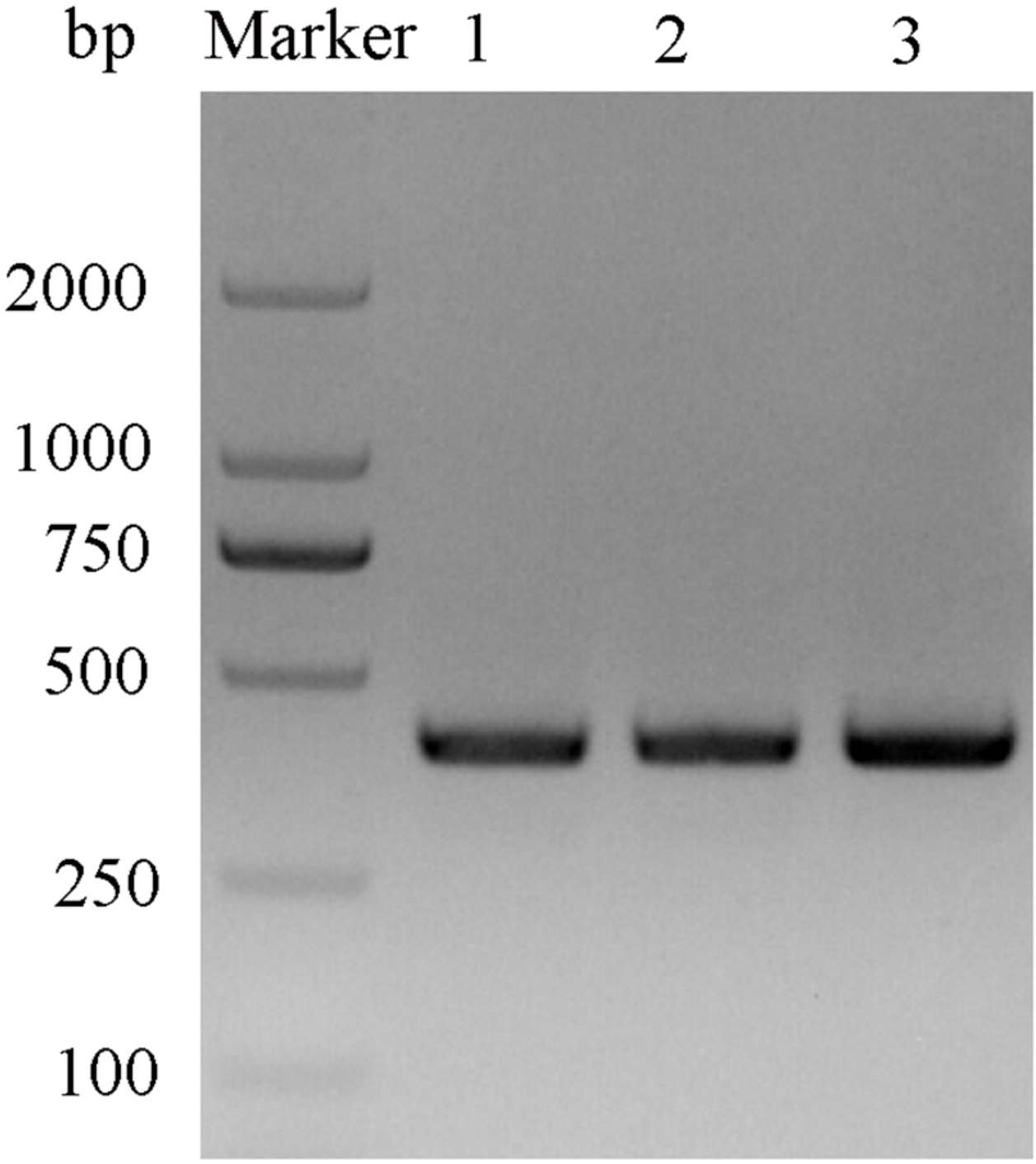
bp
Marker
1
2
3
2000
1000
750
500
250
100

Figure 4

SDS-PAGE analysis of the total bacterial protein lysate of the mutant and wild-type CbuqPBP1

(A) CbuqPBP1-His53A mutant. Lane 1: IPTG induced total protein lysate; Lane 2: total protein lysate without IPTG induction. (B) CbuqPBP1- Phe69A mutant. Lane 1: total protein lysate without IPTG induction; Lane 2: IPTG induced total protein lysate. (C) wild-type CbuqPBP1. Lane 1: IPTG induced total protein lysate; Lane 2: total protein lysate without IPTG induction.

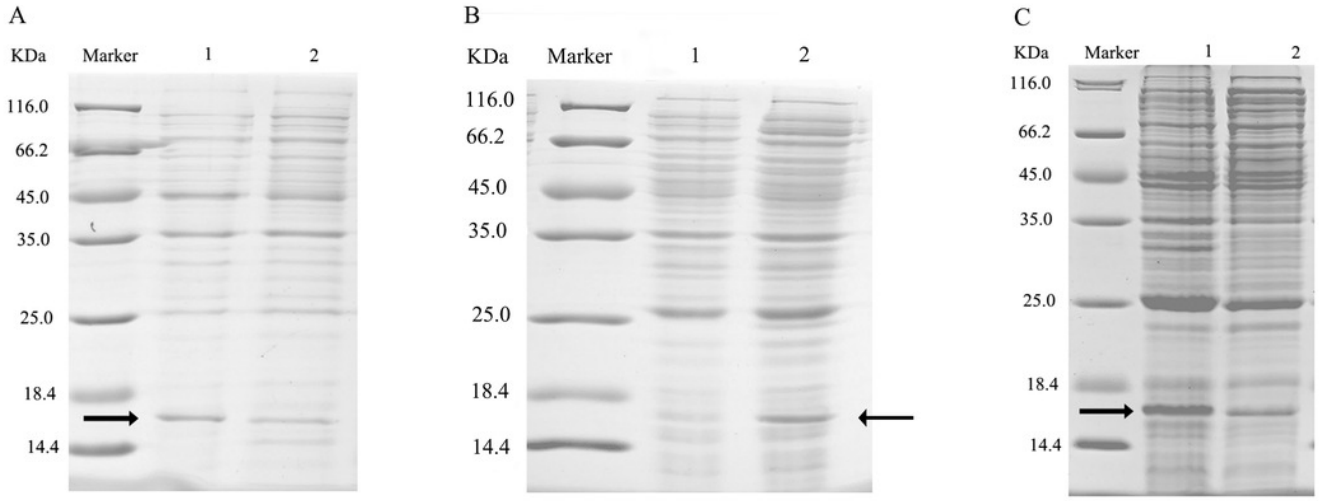

Figure 5

SDS-PAGE analysis of supernatant and precipitant of bacterial fragmentation following expression of the mutant and wild-type CbuqPBP1

Lane 1: IPTG induced expression of insoluble material; Lane 2: IPTG induced expression of supernatant following cell disruption by sonication. (A) wild-type protein. (B) CbuqPBP1-His53A mutant. (C) CbuqPBP1- Phe69A mutant.

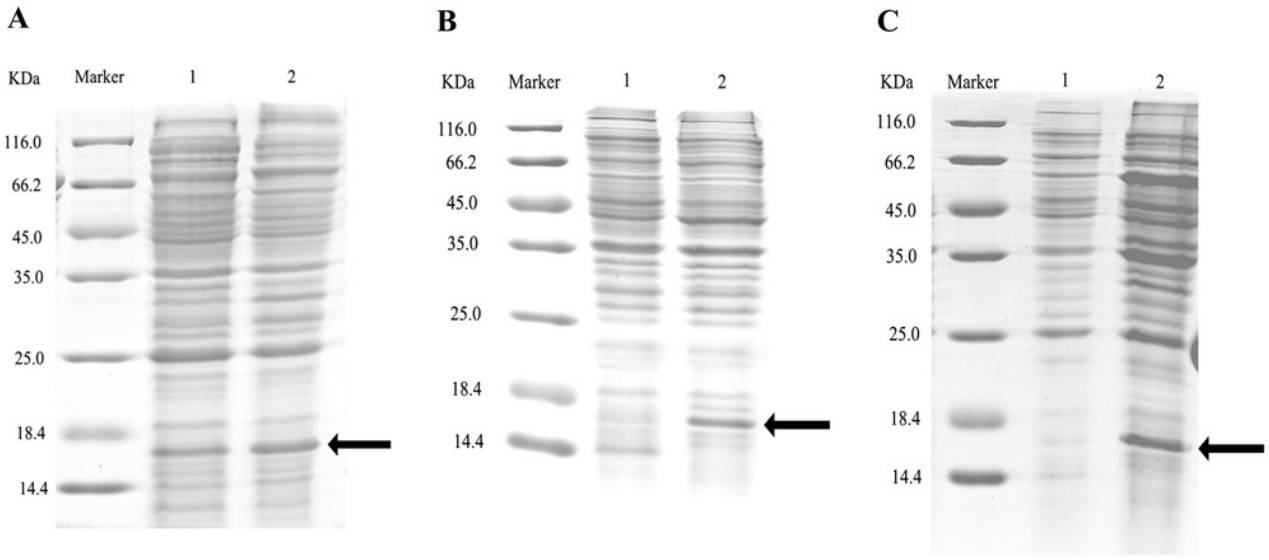

Figure 6

The binding curve and K_d of mutant and wild-type CbuqPBP1 toward 1-NPN

(A) wild-type protein. (B) CbuqPBP1-His53A mutant. (C) CbuqPBP1- Phe69A mutant.

A

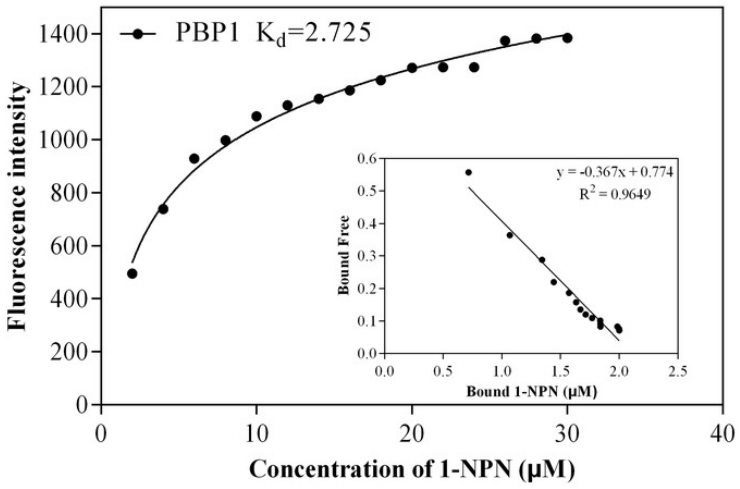
PBP1 K_d=2.725
Fluorescence intensity
Concentration of 1-NPN (μM)
y = -0.367x + 0.774
R^2 = 0.9649
Bound Free
Bound 1-NPN (μM)

B

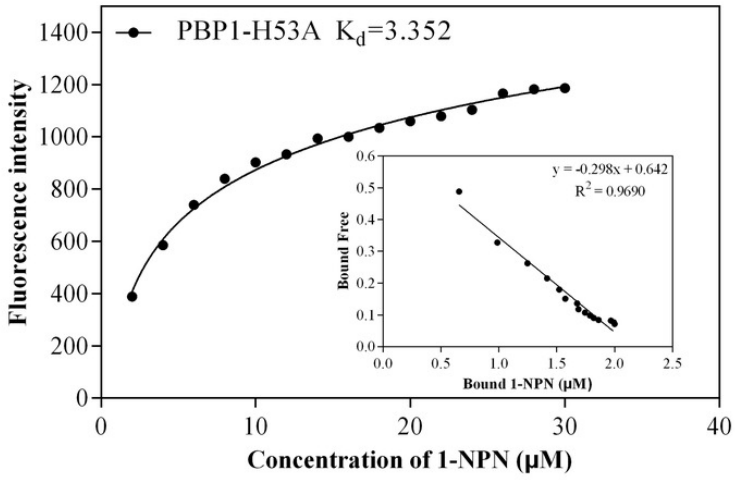
PBP1-H53A K_d=3.352
Fluorescence intensity
Concentration of 1-NPN (μM)
y = -0.298x + 0.642
R^2 = 0.9690
Bound Free
Bound 1-NPN (μM)

C

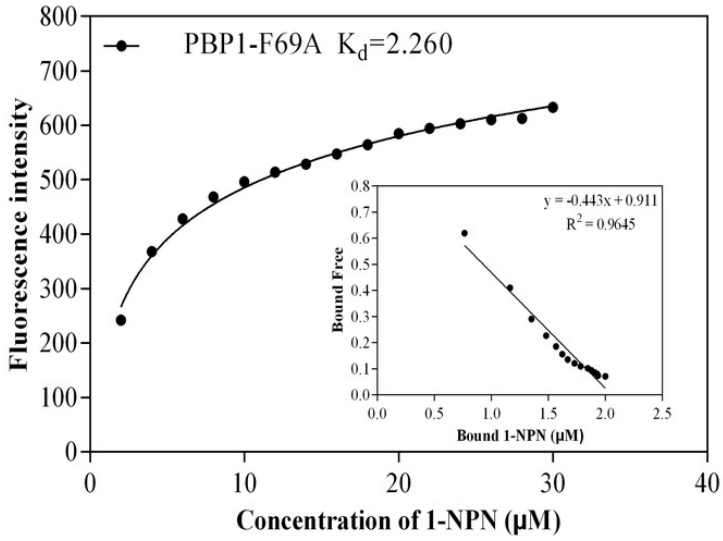
PBP1-F69A K_d=2.260
Fluorescence intensity
Concentration of 1-NPN (μM)
y = -0.443x + 0.911
R^2 = 0.9645
Bound Free
Bound 1-NPN (μM)

Figure 7

Competitive binding curves of selected ligands toward mutant and wild-type CbuqPBP1

(A) wild-type protein. (B) CbuqPBP1-His53A mutant. (C) CbuqPBP1- Phe69A mutant.

A

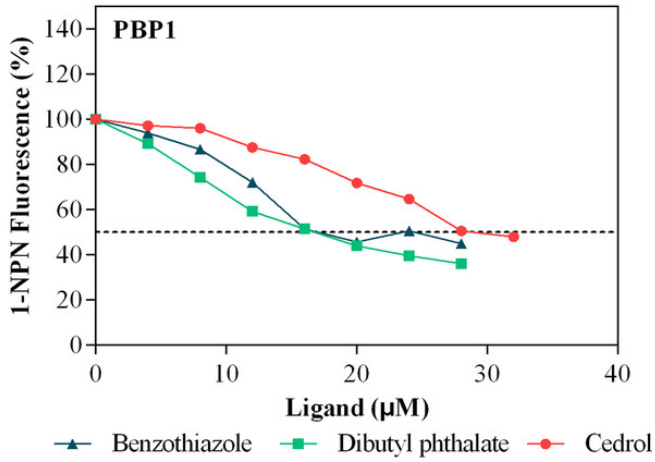
PBP1
1-NPN Fluorescence (%)
Ligand (μM)
Benzothiazole
Dibutyl phthalate
Cedrol

B

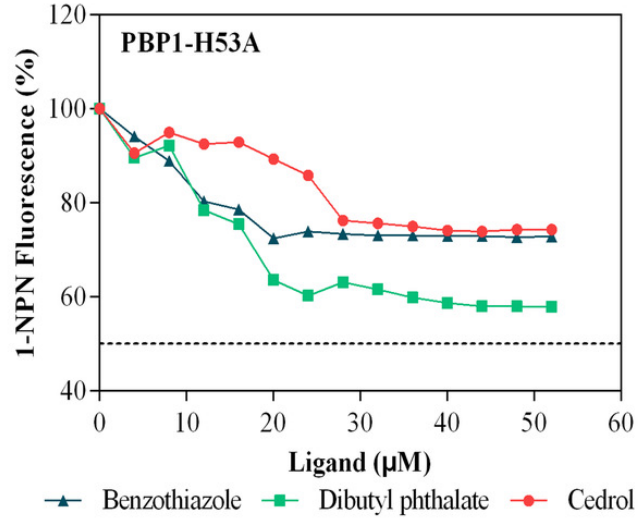
PBP1-H53A
1-NPN Fluorescence (%)
Ligand (μM)
Benzothiazole
Dibutyl phthalate
Cedrol

C

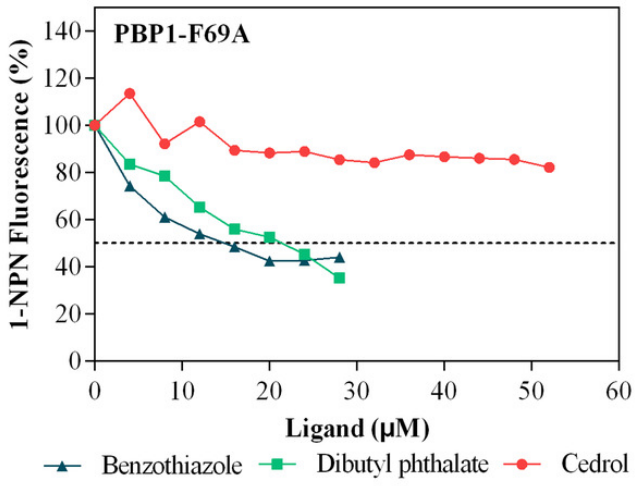
PBP1-F69A
1-NPN Fluorescence (%)
Ligand (μM)
Benzothiazole
Dibutyl phthalate
Cedrol